4-2011

Suppression Of The Plasmon Resonance In Au/cds Colloidal Nanocomposites

Elena Khon

Andrey Mereshchenko

Alexander N. Tarnovsky
Bowling Green State University, atarnov@bgsu.edu

Krishna Acharya

Anna Klinkova

See next page for additional authors

NANO LETTERS

LETTER

pubs.acs.org/NanoLett

Suppression of the Plasmon Resonance in Au/CdS Colloidal Nanocomposites

Elena Khon,[†,§] Andrey Mereshchenko,[†,‡] Alexander N. Tarnovsky,[†,‡] Krishna Acharya,[†,§] Anna Klinkova,[†,§] Nishshanka N. Hewa-Kasakarage,[§] Ian Nemitz,[§] and Mikhail Zamkov*[,†,§]

[†]The Center for Photochemical Sciences, [‡]Department of Chemistry, and [§]Department of Physics, Bowling Green State University, Bowling Green, Ohio 43403, United States

Supporting Information

ABSTRACT: The nature of exciton−plasmon interactions in Au-tipped CdS nanorods has been investigated using femtosecond transient absorption spectroscopy. The study demonstrates that the key optoelectronic properties of composite heterostructures comprising electrically coupled metal and semiconductor domains are substantially different from those observed in systems with weak interdomain coupling. In particular, strongly coupled nanocomposites promote mixing of electronic states at semiconductor−metal domain interfaces, which causes a significant suppression of both plasmon and exciton excitations of carriers.

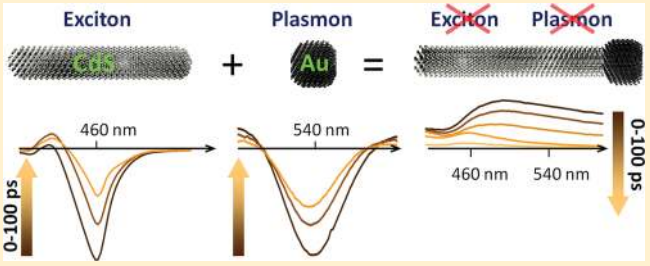

KEYWORDS: Plasmonics, photovoltaics, nanocrystals, quantum dots, nanorods

Bulk heterojunctions of metal and semiconductor materials have long been of interest to fundamental science and device engineering due to the unique interaction of respective domains through the formation of the space-charge region,[1] which gives rise to numerous technological applications including Schottky barrier solar cells,[2] solid state lasers,[3] light-emitting diodes,[4] and field effect transistors.[5] Recently, the growing ability to fabricate metal−semiconductor (M-S) composites on a nanoscale has opened up new opportunities for designing multifunctional materials with properties that cannot be obtained in the bulk phase. Over the past decade, a wide variety of nanocomposite morphologies, including metal-core/semiconductor-shell heterostructures,[6−8] metal-tipped semiconductor nanocrystals (NCs),[9−17] and organically and nonepitaxially[6,18,19] coupled metal−semiconductor composites have all been proposed for manipulating energy at nanoscale with potential utilization of these nanomaterials in areas of photovoltaics and solar fuel production,[20] lasers,[21] and Schottky detectors.[22]

Of a particular interest is a fundamental interaction between semiconductor excitons and surface plasmons (SP) of metal nanoparticles, which results from the modification of the exciton dipole moment due to local electromagnetic modes of SP.[23,24] This interaction is enabled by the nanoscopic nature of both material domains and has a unique effect on optoelectronic properties of a composite M-S system, which has been shown to dramatically alter the energy flow that occurs across M-S junctions. For instance, the presence of plasmon radiative field in metals, caused by resonant oscillations of low-energy conduction electrons, can strongly affect the dynamics of excitons in S NCs via two distinct interaction mechanisms, including plasmon−exciton energy transfer and modification of the local radiation field in S domains.

Multiple studies have explored the nature of exciton−plasmon interactions in a *weak* coupling regime, characterized by the presence of a substantial potential barrier at the interface of S and M components, which was achieved experimentally by using spacer molecules or nonepitaxial domain coupling. For these composites, the emission intensity in S domains was increased[25−32] due to the plasmon-induced enhancement of S radiative rates,[33,34] and was subsequently explored toward improving the process of light amplification in lasers.[21,35−38] Likewise, the plasmon-induced enhancement of the electric field in S domains has been demonstrated to increase the absorption cross section of S nanocrystals,[39,40] thus promoting the development of light-concentrating nanocomposites to aid the energy harvesting mechanism in photovoltaic and photocatalytic applications.[20,40] In addition to intensity enhancement, spectral modulation of the S emission in S-M composites has also been utilized for sensing target proteins attached to the linker moiety in Au-CdTe assemblies.[41] Finally a weak exciton−plasmon interaction, achieved through nonepitaxial coupling of M and S domains using a core/shell morphology, has been employed for controlling the spin of Au nanoparticles,[18] with potential utilization of this phenomenon in quantum information and spintronics.[42−44]

When metal and semiconductor components are coupled directly, without using a spacer moiety, the potential barrier for charges residing in adjacent domains may become sufficiently small to allow interdomain charge transfer and associated mixing of electronic states at the M-S interface. In addition, the enhanced

Received: February 3, 2011
Revised: March 14, 2011
Published: March 21, 2011

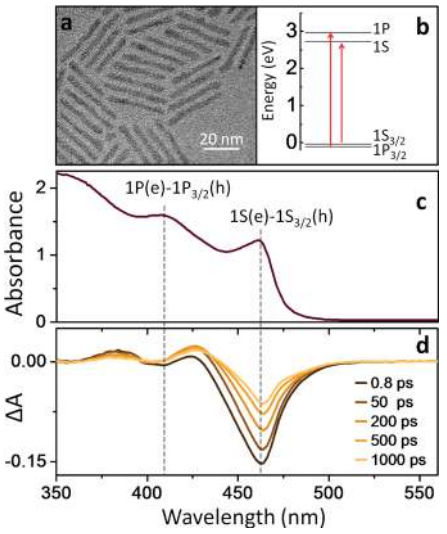

Figure 1. (a) A typical TEM image of "pure" CdS nanorods used for seeding the growth of Au domains. (b) Energy diagram showing the two lowest-energy transitions in CdS NRs, corresponding to the excitation of $1S(e)-1S_{3/2}(h)$ and $1P(e)-1P_{3/2}(h)$ excitons, distinguishable in the absorbance spectra of CdS NRs (c) as the two broad-range peaks. (d) Temporal changes in the absorbance of CdS NRs induced by 340 nm excitation pulses. The negative signal around $\lambda \approx 465$ nm, known as spectral bleach, is produced by the excitation of $1S(e)1S_{3/2}(h)$ transitions, while a smaller negative signal at $\lambda \approx 410$ nm corresponds to the formation of $1P(e)1P_{3/2}(h)$ excitons.

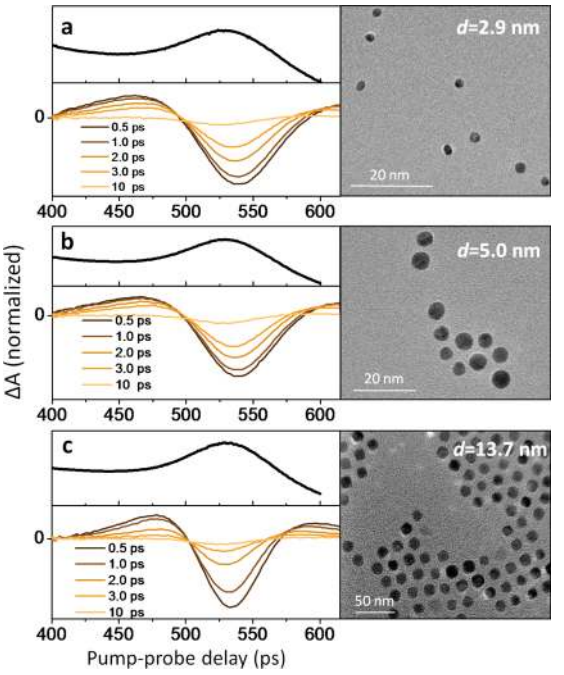

Figure 2. Steady-state and transient absorption spectra of isolated Au domains, corresponding to three different nanoparticle sizes: (a) 2.9 nm; (b) 5.0 nm; (c) 13.7 nm.

electromagnetic field of M plasmons in such strong coupling mode may produce further modifications of carrier dynamics associated with shared oscillations of the excitation energy between S and M domains, often referred to as Rabi oscillations.[45] In line with these expectations, several recent experimental reports[9,11,17] have indicated that directly coupled M-S nanocomposites exhibit optoelectronic properties that are dramatically different from those of isolated M and S nanoparticles and are often overlooked by existing theoretical models, which calls into question the nature of exciton−plasmon interactions in *epitaxial* M-S nanocomposites. For instance, it has been reported[46] that a direct growth of Au tips onto S nanorods leads to quenching of the fluorescence in the S domain due to an ultrafast transfer of excited electrons into Au. However, an alternative explanation based on the existence of sub-band gap states at the M-S interface cannot be ruled out. Furthermore, there is essentially no theoretical account for the energy-dependent changes in the absorbance profile of the S component arising as a result of direct coupling to a M domain. Explaining these phenomena requires a deeper understanding of underlying electron processes that take place in strongly coupled M-S nanocomposites and would aid the formulation of design principles necessary for the implementation of *epitaxial* M-S nanocomposites in future nanoelectronic device architectures.

Here, we employ femtosecond transient absorption spectroscopy to investigate the dynamics of exciton−plasmon interaction in epitaxial composites of Au and CdS nanoparticles representing a case of strong domain coupling. We find that plasmon oscillations in Au are strongly damped due to the presence of S domains, which is attributed to mixing of M and S electronic states. We also show that electron transfer from CdS to Au domain occurs at a rate which is slower than quenching of FL in the semiconductor component and thus cannot be used to explain the commonly observed suppression of FL emission in Au/CdS nanocomposites. Instead, present measurements indicate that the formation of excitons and corresponding band gap emission in CdS are suppressed as a result of ultrafast carrier trapping by the interfacial states. Finally, we propose that charging of gold domains under illumination effectively decreases the quantum confinement of CdS nanorods, which explains previously observed modification of CdS spectra in M-S nanocomposites.

Overall, the unique result revealed by ultrafast measurements is the demonstration of the spectroscopic evidence that optical signatures of isolated semiconductor (CdS) and metal (Au) domains are strongly modified in M-S systems exhibiting direct coupling of both domains. This is accompanied by the onset of new optical features, not present in weakly coupled M-S composites that include broad-range photoinduced absorption, plasmon damping, and delocalization of S excitations into Au domains, all of which may be important for the development of novel device technologies.

To better understand the nature of interaction between CdS and Au domains, we first re-examine the optical properties of isolated Au and CdS nanocrystals. Figure 1 shows the absorbance spectra of CdS nanorods fabricated via known seeded-type colloidal methods.[47−49] The spatial confinement of optical excitations in the transverse direction of CdS rods gives rise to a characteristic excitonic edge around 465 nm, which corresponds to the lowest energy transition, $1S(e)-1S_{3/2}(h)$, in these nanostructures.[50] The sharpness of the absorption edge in Figure 1c confirms a narrow dispersion of nanorod widths, which agrees well with corresponding statistical distribution obtained from transmission electron microscopy (TEM) images of these structures (Figure 1a).

The chirp-corrected transient absorption (TA) spectra (Figure 1d), resulting from the excitation of pure CdS NRs with 120 fs laser pulses (λ_{exc} = 340 nm), show an expected bleach of $1S(e)-1S_{3/2}(h)$ transitions, as well as smaller-amplitude bleach,

dx.doi.org/10.1021/nl200409x |*Nano Lett.* 2011, 11, 1792–1799

corresponding to higher energy excitations of $1P(e)-1P_{3/2}(h)$ excitons. Spectral distortion of TA traces associated with the Shark effect[51] were not observed in these measurements due to fairly low excitation intensities, corresponding to linear power dependence regime (see Figure SF1 in the Supporting Information). A negligible contribution of the Stark effect into the observed bleach dynamics is also consistent with the absence of a positive TA signal at early probe times (τ < 1 ps). The observed changes in the absorption of CdS nanocrystals (ΔA) are dominated by photoinduced electrons, as expected due to comparatively low effective masses of these carriers in bulk CdS[52,53] and high degeneracy of hole states in CdS NCs. The recovery of $1S(e)-1S_{3/2}(h)$ bleach is driven both via the radiative decay mechanism and trapping of excited carriers on nanorod surfaces, such that approximately half of the initial carrier population in the 1S(e) excited state is recovered after 300 ps, as was reported previously for isolated CdS NRs.[54]

The absorption spectra of *isolated* Au nanoparticles are examined in Figure 2. Since the excitation of surface plasmons in metals is a resonant process, its frequency is dependent on the composition, size, and shape of metal nanoparticles, as well as their dielectric environment. To get a better understanding of how the size of Au nanoparticles affects the transient and steady-state absorption of SP, samples comprising three different Au nanoparticle diameters were compared. Furthermore, to facilitate a fair comparison, the range of Au nanoparticle diameters for these measurements was chosen to overlap with the size range of Au domains in investigated heteroepitaxial Au/CdS nanocomposites. According to Figure 2, the plasmon resonance is manifested in all three samples of isolated Au nanoparticles through the pronounced broad-range absorption peak in the steady-state spectra with corresponding maxima near 530 nm. A moderate variation in the spectral position of the plasmon resonance between the three measurements is consistent with the size-dependent trend of plasma oscillations according to Mie theory.[55]

The transient absorption spectra of isolated Au colloids (λ_{exc} = 400 nm) representing the same three nanoparticle diameters show a pronounced bleach, which spectral range overlaps the steady-state absorption maxima. This negative ΔA signal in TA spectra of isolated Au nanoparticle has been previously attributed to the excitation-induced broadening of the plasmon peak, which causes the TA spectra to form a characteristic "dip" at the plasmon wavelength sandwiched by the two positive wings.[56,57] Such broadening of the plasmon absorbance results from nondipolar plasma oscillations (quadruple) in Au nanoparticles induced by the excitation pulse.[56] Notably, the central dip in the transient spectra is observed for all investigated gold samples, which further confirms the presence of resonant excited carrier oscillations in these nanoparticles.

To study the exciton−plasmon interaction in Au/CdS composites, gold domains were grown directly onto colloidal CdS NRs using a colloidal technique recently developed in our group,[16] which relies on the temperature-controlled reduction of Au−oleate complexes on semiconductor surfaces. Arguably, this method could be used to enable an advanced control of Au/CdS morphology and is expected to increase the area of Au/CdS interfaces exhibiting epitaxial associations, as compared to previously reported protocols[9] utilizing room-temperature deposition of Au tips onto cadmium chalcogenides in dodecyldimethylammonium bromide/dodecylamine mixture. The details of synthetic procedures for fabrication of Au/CdS nanocomposites comprising three different Au diameters are provided in the Supporting Information. Typically, to grow

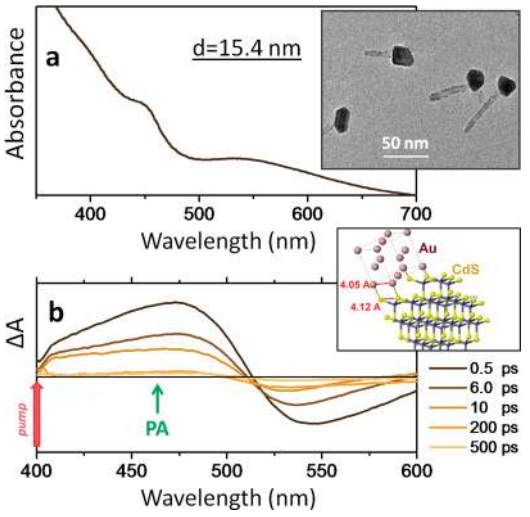

Figure 3. (a) Steady-state absorption of Au/CdS heterostructures comprising 15.4 nm Au domains. A representative TEM image is shown in the insert. (b) Transient absorption spectra of 15.4 nm Au/CdS nanocomposites resulting from the excitation at λ = 400 nm with 120 fs pump pulses. The recovery of ΔA shows an expected plasmonic feature, which resembles the corresponding TA dynamics of isolated Au nanoparticles. Surprisingly, bleaching of lowest-energy excitons in CdS domains is not observed for any pump−probe delay.

small-diameter Au tips on CdS NRs, 20 mg of washed CdS NRs in hexane was injected into a mixture containing 11.3 mg of $AuCl_3$ and 3 mL of degassed oleylamine. Subsequently the temperature of the solution was increased to 115 °C at a rate of 2 deg/min. To synthesize large-diameter Au domains, the amount of gold precursor was increased to 20 mg and the heating was terminated at T = 140 °C. TEM images of Au/CdS nanocomposites for each of the three samples are shown as inserts in corresponding TA spectra.

The dynamics of exciton−plasmon interactions in epitaxially coupled Au/CdS composites was first investigated for heterostructures comprising large-diameter Au nanocrystals (d = 15.4 nm), grown on one end of a CdS nanorod via a "matchstick" composite morphology (see Figure 3). The existence of epitaxial relationships between gold and semiconductor domains, with the possibility of some interfacial defects was deduced from (i) X-ray powder diffraction (XRD) measurements exhibiting no evidence of lattice alloying (see Figure SF2, Supporting Information) and (ii) high-resolution TEM images showing regular lattice fringes at the Au/CdS interface and crystallographic analysis revealing low-stress stoichiometric associations of the two crystals phases. To achieve an efficient excitation of carriers in both domains of the heterostructure, the wavelength of excitation pulses was set to 400 nm, whereby delivering sufficient photon energy for the simultaneous excitation 1S excitons in CdS (λ = 465 nm) and plasmons in Au domains (λ = 530 nm).

The TA spectra of Au/CdS matchsticks in Figure 3b shows spectrally broad bleaching of the absorption profile around λ = 540 nm, which corresponds to plasmon oscillations in Au domains (note that x scales in (a) and (b) are different). The intensity of this bleach reaches its maximum in less than 500 fs, driven primarily by excitations of hot carriers and simultaneous fast cooling of the nonequilibrium carrier population via electron−electron interaction, and subsequently recovers to $\Delta A(\lambda) = 0$ in 500 ps. While the observed plasmon bleaching kinetics is in line with the TA spectra of isolated Au nanoparticles, surprisingly, there is no evidence of the

dx.doi.org/10.1021/nl200409x |*Nano Lett.* 2011, 11, 1792–1799

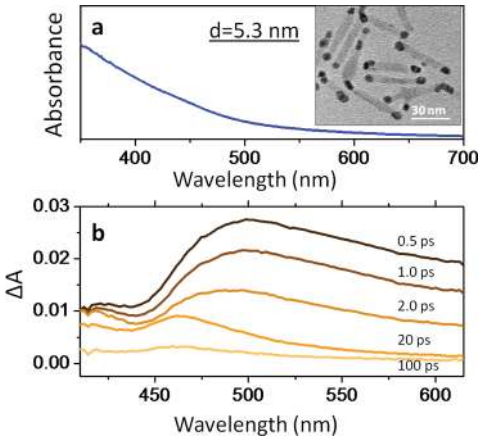

Figure 4. (a) Steady-state absorption of Au/CdS heterostructures comprising 5.3 nm Au domains. A representative TEM image is shown in the insert. (b) Temporal evolution of the TA spectra for 5.3 nm Au/CdS nanocomposites excited at $\lambda = 400$ nm. The TA trend contrasts the recovery dynamics observed in isolated Au and CdS nanoparticles, for which both excitonic and plasmonic features are manifested by the prominent dip in ΔA. Instead, the value of ΔA observed for Au/CdS nanocomposites remains positive throughout the entire spectral range of the probe beam.

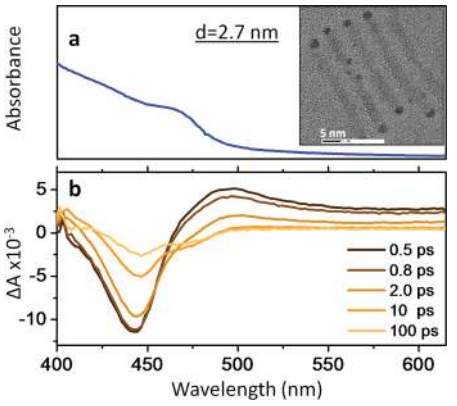

Figure 5. (a) Steady-state absorption of Au/CdS heterostructures comprising 2.7 nm Au domains (a typical TEM image is shown in the insert). (b) Temporal evolution of the TA spectra for 2.7 nm Au/CdS nanocomposites resulting from the excitation at $\lambda = 400$ nm with 120 fs pump pulses. The negative ΔA signal at $\lambda \approx 445$ nm corresponds to bleaching of band gap transitions in CdS. Its spectral position is blue-shifted from the corresponding excitonic edge in the steady-state spectrum, which is believed to be caused by the positive contribution of the photoinduced absorbance into Δ A at the low-energy side of the excitonic peak. The absence of the plasmon bleach at $\lambda = 560$ nm is interpreted as a suppression of plasmon oscillations.

TA bleach at 465 nm, corresponding to the formation of excitons in the CdS domain of the heterostructure. In contrast to the TA profile of pure CdS NRs, showing a well-defined $1S(e)-1S_{3/2}(h)$ bleach ($\Delta A/A = -0.15$), the TA amplitude of Au/CdS nanocomposites in the same wavelength range is positive (green arrow in Figure 3b)!

The absence of a distinct excitonic feature corresponding to $1S(e)-1S_{3/2}(h)$ transitions in Au/CdS composites can explain the observed quenching of FL emission in S domains, which was also reported by other studies, wherein metal tips were grown directly onto the S component via colloidal routes.[9,58−61] However, a generally accepted explanation attributing the FL quenching in S domains to the photoinduced transfer of 1S(e) electrons into Au does not seem to be compelling in light of the full suppression of the CdS bleach. Indeed, if an electron transfer was the dominant mechanism depleting the population of 1S(e) states in CdS, a significant portion of excited electrons would still be present in the 1S(e) state after 500 fs, since the transfer of carriers across nanoscale inorganic interfaces is generally slow enough to be observed using TA spectroscopy (τ(e) > 350 fs, τ(h) > 650 fs).[54,62−67] Furthermore, an electron transfer process by itself, cannot account for an onset of a positive TA signal spanning a broad wavelength range from 400 to 520 nm, which was not present in the TA spectra of isolated Au and CdS domains. We note however, that decay of this positive TA feature can provide some clues regarding the origin of microscopic processes underpinning the carrier dynamics in Au/CdS nanocomposites, as its slow recovery (>100 ps) strongly suggests a contribution from the photoinduced absorption (PA) of excited carriers in either Au or CdS domains.

Overall, the observed TA spectra of Au/CdS composites comprising a large-diameter gold domain (Figure 3) are qualitatively different from those of isolated Au and CdS nanoparticles, as manifested both by the absence of bleaching signal in the semiconductor component, photoinduced absorption, and by the relatively weak bleaching of the SP feature in Au. To get a deeper insight into the origin of this complex carrier dynamics, Au/CdS heterostructures comprising smaller size Au domains were examined next.

Figure 4 shows the TA spectra of Au/CdS heterostructures comprising 5.3 nm Au nanoparticles. For these nanocomposites, bleaching of the SP resonance in Au domains is no longer distinguishable, which strongly contrasts the TA dynamics of isolated nanoparticles (see Figure 1) exhibiting an apparent plasmon bleach at $\lambda = 530$ nm. The SP peak is also missing from the steady-state absorption spectrum of Au/CdS nanocomposites, even though this feature is clearly present in the absorption profile of isolated Au nanoparticles, indicating that the nature of excited electron oscillations in Au domains is modified due to direct coupling of CdS NCs. In addition to the suppressed SP feature, TA spectra in Figure 4 reveal a broad positive signal, which, in comparison with a TA trend of 15.4 nm Au/CdS heterostructures, extends across the entire spectral window of the probe pulse. The recovery of this feature is too slow to be classified as a nonlinear modification of the spectral profile due to local fields and, similar to the case of 15.4 nm Au/CdS heterostructures, was attributed to the photoinduced absorption of excited carriers occupying electronic states within CdS band gap. Interestingly, decreasing the size of gold domains from 15.4 to 5.3 nm results in the appearance of an S excitonic feature, which is manifested by a characteristic dip at $\lambda <$ 450 nm, corresponding to the excitation of ground-state excitons, $1S(e)-1S_{3/2}(h)$. Notably, the observed excitonic bleach is substantially weaker than that of pure CdS NRs and is offset by the positive background of the broad photoinduced absorption.

To uncover further experimental facts promoting the explanation of the observed plasmon suppression and photoinduced absorption in Au/CdS nanocomposites, we turn to the next structural morphology of Au/CdS composites, for which the size of Au domains is only 2.7 nm (Figure 5). These heterostructures were chosen as a transitional system spanning the link between optical properties of pure CdS nanorods and those of 5.3 nm Au/CdS nanocomposites, which exhibit several "unusual" trends, including suppression of the plasmon bleach, suppression of excitonic features in CdS, and spectrally broad photoinduced absorption.

dx.doi.org/10.1021/nl200409x |*Nano Lett.* 2011, 11, 1792–1799

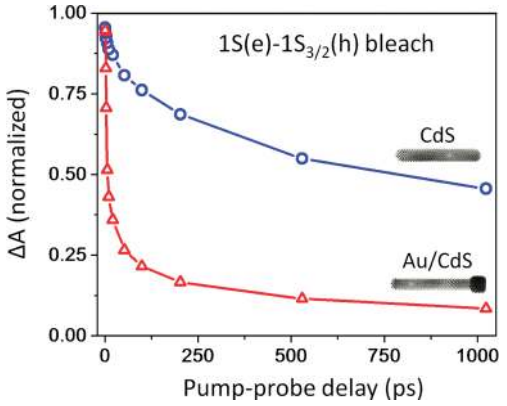

Figure 6. Temporal evolution of 1S(e)−1S(h) excitons in "pure" CdS NRs (blue) and Au/CdS (red) heterostructures. A faster recovery of band edge excitons in Au/CdS ($\tau_{Au/CdS}$ = 11 ps, τ_{CdS} = 1 ns) is attributed to the transfer of 1S electrons into gold domains.

Similar to 5.3 nm Au/CdS heterostructures, transient absorption spectra of Au/CdS nanocomposites comprising 2.7 nm Au tips (Figure 5b) do not reveal any evidence of spectral bleaching in the λ = 530 nm range, corresponding to the excitation-induced broadening of the SP peak. Just as in the case of nanocomposites with larger tip sizes, the suppression of SP in 2.7 nm Au/CdS heterostructures contrasts the carrier dynamics observed for the control sample of isolated 2.7 nm Au nanoparticles (Figure 2), for which the presence of the plasmon resonance was manifested both through steady-state and time-resolved absorption measurements.

While SP excitations are not distinguishable in the TA spectra of 2.7 nm Au/CdS heterostructures, bleaching of excitonic transitions in the S portion of composite nanoparticles is the most pronounced of all three investigated nanocomposite morphologies, with the observed ΔA profile being nearly identical to that of pure CdS NRs. Notably, the decay of CdS excitons in 2.7 nm Au/CdS nanocomposites occurs an order of magnitude faster than those in pure CdS NRs, as was estimated from the comparison of respective decay traces in Figure 6, and is attributed to the transfer of photoinduced carriers from CdS into Au domains. Such charge transfer kinetics is consistent with the previously measured interdomain carrier transfer dynamics in epitaxial nanocomposites of the two semiconductor domains, for which electron transition times of 350 fs[54] were reported. A slower transfer of photoinduced carriers at the Au/CdS interface as compared to those of semiconductor−semiconductor composites is expected due to stress-related interfacial defects and nonmatching electron momenta in adjacent crystal lattices. Finally, the amplitude of the photoinduced absorption (the positive portion of the TA signal) in 2.7 nm Au/CdS nanocomposites was found to be substantially weaker than in 5.3 nm Au/CdS heterostructures, as can be inferred from the relatively small area of the two PA cusps in Figure 5b. This positive ΔA signal is yet distinctly different from the TA profile of pure CdS NRs, which does not contain positive "wings" (Figure 1d), or SP excitations in Au domains, which contribute a positive ΔA only at substantially lower energies (Figure 2). Therefore, the PA signal of Au/CdS nanocomposites is believed to arise as a result of direct coupling between M and S domains that mutually create a modified distribution of electronic states, allowing for the excitation of low-energy conduction electrons contributing into PA.

The TA dynamics of investigated Au/CdS nanocomposite morphologies shows several important trends. First, the plasmon

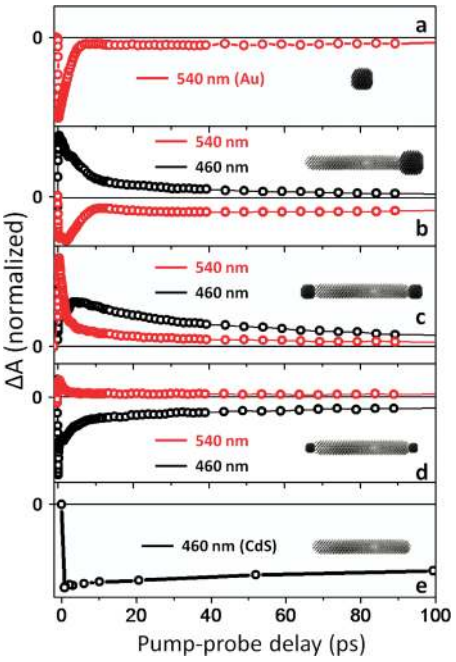

Figure 7. The kinetics of bleach recovery corresponding to exciton (λ = 460 nm, black curve), and plasmon (λ = 540 nm, red curve) excitations observed for (a) isolated gold nanoparticles, (b) 15.4 nm Au/CdS heterostructures, (c) 5.3 nm Au/CdS heterostructures, (d) 2.7 nm Au/CdS heterostructures, and (e) "pure" CdS nanorods.

absorption in Au/CdS heterostructured is suppressed. This effect is particularly strong in heterostructures comprising small-diameter Au, for which any spectral features associated with SP oscillations are completely vanished from the TA spectra (Figure 7). Such suppression of Au/CdS plasmons is clearly conflicting the measurements of SP in isolated gold nanoparticles, which show both the transient and steady-state signatures of the SP resonance. Second, there is a strong suppression of excitonic features in CdS domains, with the magnitude of this effect exhibiting positive correlation with the size of the Au domain. As demonstrated above, this suppression cannot be explained in terms of photoinduced transfer of charges from CdS to Au domains. Third, TA spectra of all Au/CdS nanocomposites show strong photoinduced absorption, which is not present in the spectra of isolated CdS and Au components, as evident from kinetic traces in Figure 7.

To explain the observed suppression of SP oscillations in Au domains, we consider a "low-barrier" coupling between Au and CdS components, for which Au electrons with energies located above the Fermi level (plasmon band) are not sufficiently confined by the Au/CdS interface to exhibit resonant oscillations. The validity of this assumption is supported by the fact that the interface of the two nanosized domains consists of just a few monolayers and thus cannot form a substantial potential barrier and the fact that energies of conduction electrons in Au domains are raised relative to their respective positions in isolated Au nanoparticles due to charging. Indeed, the photoinduced transfer of excited electrons from CdS to Au (see Figure 6) leaves Au domains with an excess negative charge, which equalizes the energy difference between the conduction states in both domains.[68] As a result, electronic wave functions of conduction carriers in S and charged M domains partly overlap, giving rise to mixing of electronic states at the interface and corresponding changes in the density of states in both materials (see Figure 8). For small-diameter Au nanoparticles, such mixing

dx.doi.org/10.1021/nl200409x |Nano Lett. 2011, 11, 1792–1799

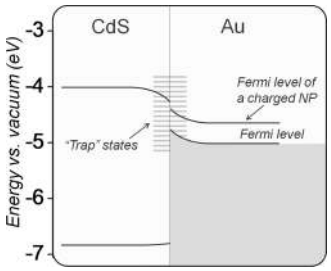

Figure 8. Energy diagram showing the effect of strong interdomains coupling on electronic energies in Au/CdS heterostructures, which gives rise to the onset of new electronic states. First, the interface of Au and CdS materials can support the formation of trap states, whose energies are located between the Fermi level of Au nanoparticles and the conduction band of CdS NCs. Photoinduced filling of these states is manifested by the spectrally wide photoinduced absorption signal observed in TA measurements. Second, excitation bands of both Au and CdS domains are "bent" at the interface similar to those of bulk heterostructures to account for delocalization of carriers across interdomain boundary.

results in the delocalization of the plasma electrons into CdS portion of nanocomposites, which has a substantially greater volume and therefore can significantly reduce the boundary effect in Au nanoparticles. Such delocalization-induced suppression of the plasmon resonance in Au NPs is further supported by steady-state absorption spectra of 2.7 and 5.3 nm Au/CdS nanocomposites through the absence of distinct plasmon features. These time-independent measurements rule out nonlinear excitation effects as a potential origin of plasmon suppression since excitation intensities used in steady-state absorption experiments are orders of magnitude below those used in ultrafast studies.

The proposed mixing of the electronic states at the interface of Au and CdS domains can also explain the existence of a positive TA signal observed for all investigated Au/CdS heterostructures. Indeed, due to strong coupling of S and M domains, carrier excitations in CdS can lead to the population of CdS-modified conduction states of Au, which will then serve the role of interfacial trap states (schematically shown in Figure 8). This process can occur on a time scale faster than the pulse duration, as can be expected from the general nature of excitation processes in nanocrystals,[69] and will therefore contribute into the "instantaneous" photoinduced absorption of Au/CdS nanocomposites, manifested by the positive ΔA. A relatively large amplitude of this process is attributed to the fact that in addition to facet-localized Au tips, CdS NRs contain a range of smaller gold domains attached to NR walls that can crate electron traps along the surface. Notably, for matchstick samples, exhibiting a relatively small interfacial area due to one-side capping and the absence of side-wall defects, the PA signal is decreased. Finally, we note that a spectrally broad TA signal associated with the these traps, ($450 < \lambda < 625$ nm, for 5.3 nm Au/CdS), results from an expected wide dispersion of electronic energies in Au and the fact that energies of excited carriers in Au domains are shifted upward from their positions in bulk Au due to charging.

While the suppression of plasmons in Au domains can be explained in terms of delocalization of conduction states across the Au/CdS interface, the absence of the excitonic features in the TA and steady-state spectra can, likewise, be attributed to tunneling of CdS carriers into Au domains. Indeed, for small-diameter Au tips, the delocalization of CdS electrons into M is limited to a few nanometers, which is insufficient to alter the character of quantum confinement in CdS, as can be confirmed by nearly unsuppressed CdS bleach in 2.7 nm Au/CdS spectra (Figure 5b), meanwhile, large-size Au domains allow for a substantial delocalization of 1S(e) CdS wave functions into metal, thus leading to the suppression of excitonic features. Expectedly, the correlation between the degree of exciton suppression and the size of Au domains is opposite to that of plasmon suppression, which is the strongest when the size of Au tips is the smallest.

To provide a consistent picture of electron transitions in a directly coupled Au/CdS system, we propose a simple model of interfacial state mixing, which can be viewed as a nanoscale analogue of the depletion region observed in bulk M-S composite films. First, we assume that the boundary of Au and CdS materials can support interfacial states or electron traps, as illustrated in Figure 8, forming as a result of mismatching lattice types and the apparent proximity between electronic energies of CdS and Au conduction states. Energies of excited carriers occupying these states are uniformly distributed between the Fermi level of Au and the conduction band of CdS (see Figure 8) and, therefore, can explain the observed long-lived PA feature. Such contribution of interfacial states into ultrafast carrier dynamics is expected to depend on the morphology of the Au/CdS interface and, in principle, could be tuned by changing the density of Au domains attached to NR surfaces. Second, we assume that the potential barrier for Au electrons at the Au/CdS interface is sufficiently small to allow the delocalization of plasma electrons into CdS. As a result, the dielectric function at the boundary of Au and CdS domains changes from imaginary (gold) to real and positive (semiconductor) continuously rather than sharply (Figure 8), which, in agreement with the Mie theory, results in quenching of plasmonic oscillations. This assumption is supported by the fact that plasmon suppression is stronger for heterostructures with smaller Au domains, for which a significant portion of domain surfaces is adjacent to CdS, promoting the delocalization of conduction electrons.

In summary, femtosecond transient absorption spectroscopy was used to investigate the nature of exciton−plasmon interactions in epitaxially coupled Au/CdS nanocomposites. It was shown that mixing of conduction states at the interface of metal and semiconductor domains leads to the onset of unique optoelectronic properties, which are not observable in nonepitaxial metal−semiconductor heterostructures. One of these properties is the complete suppression of surface plasmon oscillations in Au domains, which is attributed to the delocalization of plasma electrons into CdS portion of the structure. Careful analyses of the transient kinetics as well as steady-state absorption data revealed that resonant plasmon oscillations are quenched in nanocomposites comprising small-diameter Au domains (<6 nm), which contrasts the plasmon dynamics in weakly coupled M-S systems. In addition to plasmon suppression, we also find that the formation of bound electron−hole pairs (excitons) in CdS portion of the structure is strongly hindered due to the presence of gold domains. This phenomenon is explained here in term of the proposed mixing of conduction states at the boundary of M and S materials, which creates favorable conditions for valence electrons in CdS to be excited directly into interfacial states thus lowering the probability of band gap transitions. By using ultrafast spectroscopy, we demonstrate that it is the proposed interdomain mixing of electronic states and not the electron transfer process that leads to FL quenching in CdS domains. Further support of the proposed interfacial state mixing is provided by the observation of a characteristic, long-lived photoinduced absorption (positive TA signal), which confirms the interfacial character of excited states in Au/CdS heterostructures.

dx.doi.org/10.1021/nl200409x |*Nano Lett.* 2011, 11, 1792–1799

■ ASSOCIATED CONTENT

Supporting Information. Experimental details and the excitation power dependence measurements. This material is available free of charge via the Internet at http://pubs.acs.org.

■ AUTHOR INFORMATION

Corresponding Author
*E-mail: zamkovm@bgsu.edu.

■ ACKNOWLEDGMENT

We gratefully acknowledge Bowling Green State University for financial support (SF07, RIC2009, RCE2009).

■ REFERENCES

(1) Many, A.; Goldstein, Y.; Grover, N. B. *Semiconductor Surfaces*; North Holland: Amsterdam, 1965.
(2) Loutfy, R. O.; Sharp, J. H. *J. Am. Chem. Soc.* **1979**, *71*, 1211–1217.
(3) Nolte, D. D. *J. Appl. Phys.* **1999**, *85*, 6259–6289.
(4) Ozgur, U.; Alivov, Y. I.; Liu, C.; Teke, A.; Reshchikov, M. A.; Dogan, S.; Avrutin, V.; Cho, S. J.; Morkoc, H. *J. Appl. Phys.* **2005**, *98*, No. 041301.
(5) Storm, H. F. *IEEE Trans. Electron Devices* **1969**, *ED16*, 957.
(6) Zhang, J. T.; Tang, Y.; Lee, K.; Ouyang, M. *Science* **2010**, *327*, 1634–1638.
(7) Shi, W. L.; Zeng, H.; Sahoo, Y.; Ohulchanskyy, T. Y.; Ding, Y.; Wang, Z. L.; Swihart, M.; Prasad, P. N. *Nano Lett.* **2006**, *6*, 875.
(8) Kim, H.; Achermann, M.; Balet, L. P.; Hollingsworth, J. A.; Klimov, V. I. *J. Am. Chem. Soc.* **2005**, *127*, 544–546.
(9) Mokari, T.; Rothenberg, E.; Popov, I.; Costi, R.; Banin, U. *Science* **2004**, *304*, 1787–1790.
(10) Carbone, L.; Kudera, S.; Giannini, C.; Ciccarella, G.; Cingolani, R.; Cozzoli, P. D.; Manna, L. *J. Mater. Chem.* **2006**, *16*, 3952.
(11) Saunders, A. E.; Popov, I.; Banin, U. *J. Phys. Chem. B* **2006**, *110*, 25421.
(12) Menagen, G.; Mocatta, D.; Salant, A.; Popov, I.; Dorfs, D.; Banin, U. *Chem. Mater.* **2008**, *20*, 6900–6902.
(13) Carbone, L.; Jakab, A.; Khalavka, Y.; Sonnichsen, C. *Nano Lett.* **2009**, *9*, 3710–3714.
(14) Menagen, G.; Macdonald, J. E.; Shemesh, Y.; Popov, I.; Banin, U. *J. Am. Chem. Soc.* **2009**, *131*, 17406–17411.
(15) Mokari, T.; Costi, R.; Sztrum, C. G.; Rabani, E.; Banin, U. *Phys. Status Solidi B* **2006**, *243*, 3952–3958.
(16) Khon, E; Hewa-Kasakarage, N. N.; Nemitz, I; Acharya, K.; Zamkov, M. *Chem. Mater.* **2010**, *22*, 5929.
(17) Costi, R.; Saunders, A. E.; Banin, U. *Angew. Chem., Int. Ed.* **2010**, *49*, 4878–4897.
(18) Zhang, J. T.; Tang, Y.; Lee, K.; Ouyang, M. *Nature* **2010**, *466*, 91–95.
(19) Lee, J.; Orazbayev, A.; Govorov, A. O.; Kotov, N. A. *J. Phys. Chem. C* **2010**, *114*, 1404–1410.
(20) Morfa, A. J.; Rowlen, K. L.; Reilly, T. H.; Romero, M. J.; van de Lagemaat, J *Appl. Phys. Lett.* **2008**, *92*, No. 013504.
(21) Oulton, R. F.; Sorger, V. J.; Zentgraf, T.; Ma, R. M.; Gladden, C.; Dai, L.; Bartal, G.; Zhang *Nature* **2009**, *461*, 629–632.
(22) Jestl, M.; Maran, I.; Kock, A.; Beinstingl, W.; Gornik, E. *Opt. Lett.* **1989**, *14*, 719–721.
(23) Drexhage, K. H. *Progress in Optics*; Wolf, E., Ed.; North-Holland: Amsterdam, The Netherlands, 1974; Vol. XII, p 163.
(24) Achermann, M. *J. Phys. Chem. Lett.* **2010**, *1*, 2837–2843.
(25) Shimizu, K. T.; Woo, W. K.; Fisher, B. R.; Eisler, H. J.; Bawendi, M. G. *Phys. Rev. Lett.* **2002**, *89*, No. 117401.
(26) Farahani, J. N.; Pohl, D. W.; Eisler, H. J.; Hecht, B. *Phys. Rev. Lett.* **2005**, *95*, No. 017402.
(27) Bergman, D. J.; Stockman, M. I. *Phys. Rev. Lett.* **2003**, *90*, No. 027402.
(28) Mertens, H.; Biteen, J. S.; Atwater, H. A.; Polman, A. *Nano Lett.* **2006**, *6*, 2622–2625.
(29) Okamoto, K.; Niki, I.; Shvartser, A.; Narukawa, Y.; Mukai, T.; Scherer, A. *Nat. Mater.* **2004**, *3*, 601–605.
(30) Guo, P.-F.; Wu, S.; Ren, Q.-J.; Lu, J.; Chen, Z.; Xiao, S.-J.; Zhu, Y.-Y. *J. Phys. Chem. Lett.* **2010**, *1*, 315–318.
(31) Gryczynski, I.; Malicka, J.; Jiang, W.; Fischer, H.; Chan, W. C. W.; Gryczynski, Z.; Grudzinski, W.; Lakowicz, J. R. *J. Phys. Chem. B* **2005**, *109*, 1088–1093.
(32) Pillai, S.; Catchpole, K. R.; Trupke, T.; Zhang, G.; Zhao, J.; Green, M. A. *Appl. Phys. Lett.* **2006**, *88*, No. 161102.
(33) Muskens, O. L.; Giannini, V.; Sanchez-Gil, J. A.; Rivas, J. G. *Nano Lett.* **2007**, *7*, 2871–2875.
(34) Wang, Y.; Yang, T.; Tuominen, M. T.; Achermann, M. *Phys. Rev. Lett.* **2009**, *102*, No. 163001.
(35) Noginov, M. A.; Zhu, G.; Mayy, M.; Ritzo, B. A.; Noginova, N.; Podolskiy, V. A. *Phys. Rev. Lett.* **2008**, *101*, No. 226806.
(36) Noginov, M. A.; Zhu, G.; Belgrave, A. M.; Bakker, R.; Shalaev, V. M.; Narimanov, E. E.; Stout, S.; Herz, E.; Suteewong, T.; Wiesner, U. *Nature* **2009**, *460*, 1110–1112.
(37) Zheludev, N. I.; Prosvirnin, S. L.; Papasimakis, N.; Fedotov, V. A. *Nat. Photonics* **2008**, *2*, 351–354.
(38) Englund, D.; Fattal, D.; Waks, E.; Solomon, G.; Zhang, B.; Nakaoka, T.; Arakawa, Y.; Yamamoto, Y.; Vuckovic, J. *Phys. Rev. Lett.* **2005**, *95*, No. 013904.
(39) Schaadt, D. M.; Feng, B.; Yu, E. T. *Appl. Phys. Lett.* **2005**, *86*, No. 063106.
(40) Rand, B. P.; Peumans, P.; Forrest, S. R. *J. Appl. Phys.* **2004**, *96*, 7519–7526.
(41) Lee, J.; Hernandez, P.; Lee, J.; Govorov, A. O.; Kotov, N. A. *Nat. Mater.* **2007**, *6*, 291–295.
(42) Gupta, J. A.; Knobel, R.; Samarth, N.; Awschalom, D. D. *Science* **2001**, *292*, 2458–2461.
(43) Press, D.; Ladd, T. D.; Zhang, B.; Yamamoto, Y. *Nature* **2008**, *456*, 218–221.
(44) Berezovsky, J.; Mikkelsen, M. H.; Stoltz, N. G.; Coldren, L. A.; Awschalom, D. D. *Science* **2008**, *320*, 349–352.
(45) Gómez, D. E.; Vernon, K. C.; Mulvaney, P.; Davis, T. J. *Nano Lett.* **2010**, *10*, 274–278.
(46) Mokari, T.; Aharoni, A.; Popov, I.; Banin, U. *Angew. Chem., Int. Ed.* **2006**, *118*, 8169.
(47) Carbone, L.; Nobile, C.; De Giorgi, M.; Sala, F. D.; Morello, G.; Pompa, P.; Hytch, M.; Snoeck, E.; Fiore, A.; Franchini, I. R.; Nadasan, M.; Silvestre, A. F.; Chiodo, L.; Kudera, S.; Cingolani, R.; Krahne, R.; Manna, L. *Nano Lett.* **2007**, *7*, 2942–2950.
(48) Kirsanova, M.; Nemchinov, A.; Hewa-Kasakarage, N. N.; Schmall, N.; Zamkov *Chem. Mater.* **2009**, *21*, 4305–4309.
(49) Zhong, H.; Scholes, G. D. *J. Am. Chem. Soc.* **2009**, *131*, 9170–9191.
(50) Scholes, G. D. *ACS Nano* **2008**, *2*, 523–537.
(51) Klimov, V.; Hunsche, S.; Kurz, H. *Phys. Rev. B* **1994**, *50*, 8110–8113.
(52) *Landolt-Boernstein: Numerical Data and Functional Relationships in Science and Technology*. Group III, Condensed Matter, SubVol. C; Martienssen, W., Ed.; Springer: Verlag, 1998.
(53) Dinger, A.; Petillon, S.; Grün, M.; Hetterich, M.; Klingshirn, C. *Semicond. Sci. Technol.* **1999**, *14*, 595–598.
(54) Hewa-Kasakarage, N. N.; El-Khoury, P. Z.; Tarnovsky, A. N.; Kirsanova, M.; Nemitz, I.; Nemchinov, A.; Zamkov, M. *ACS Nano* **2010**, *4*, 1837–1844.
(55) Kreibig, U.; Vollmer, M. *Optical Properties of Metal Clusters*; Springer: Berlin, Germany, 1995.
(56) Ahmadi, T. S.; Logunov, S. L.; El-Sayed, M. A. *J. Phys. Chem.* **1996**, *100*, 8053–8056.
(57) Logunov, S. L.; Ahmadi, T. S.; El-Sayed, M. A. *J. Phys. Chem. B* **1997**, *101*, 3713–3719.

(58) Yong, K. T.; Sahoo, Y.; Choudhury, K. R.; Swihart, M. T.; Minter, J. R.; Prasad, P. N. *Nano Lett.* **2006**, *6*, 709.
(59) Pacholski, C.; Kornowski, A.; Weller, H. *Angew. Chem., Int. Ed.* **2004**, *43*, 4774.
(60) Mokari, T.; Aharoni, A.; Popov, I.; Banin, U. *Angew. Chem., Int. Ed.* **2006**, *45*, 8001.
(61) Yong, K. T.; Sahoo, Y.; Choudhury, K. R.; Swihart, M. T.; Minter, J. R.; Prasad, P. N. *Chem. Mater.* **2006**, *18*, 5965.
(62) Peng, P.; Milliron, D. J.; Hughes, S. M.; Johnson, J. C.; Alivisatos, A. P.; Saykally, R. J. *Nano Lett.* **2005**, *5*, 1809–1813.
(63) Dooley, C. J.; Dimitrov, S. D.; Fiebig, T. *J. Phys. Chem. C* **2008**, *112*, 12074–12076.
(64) Lupo, M. G.; Sala, F. D.; Carbone, L.; Zavelani-Rossi, M.; Fiore, A.; Lüer, L.; Polli, D.; Cingolani, R.; Manna, L.; Lanzani, G. *Nano Lett.* **2008**, *8*, 4582–4587.
(65) Hewa-Kasakarage, N. N.; El-Khoury, P. Z.; Schmall, N.; Kirsanova, M.; Nemchinov, A.; Tarnovsky, A. N.; Bezryadin, A.; Zamkov, M. *Appl. Phys. Lett.* **2009**, *94*, No. 133113.
(66) Hewa-Kasakarage, N. N.; Kirsanova, M.; Nemchinov, A.; Schmall, N.; El-Khoury, P. Z.; Tarnovsky, A. N.; Zamkov, M. *J. Am. Chem. Soc.* **2009**, *131*, 1328–1334.
(67) Hewa-Kasakarage, N. N.; Gurusinghe, P. G.; Zamkov, M. Blue-Shifted Emission in CdTe/ZnSe Heterostructured Nanocrystals. *J. Phys. Chem. C* **2009**, *113*, 4362–4368.
(68) Wood, A.; Giersig, M.; Mulvaney, P. *J. Phys. Chem. B* **2001**, *105*, 8810.
(69) Klimov, V. I. *Annu. Rev. Phys. Chem.* **2007**, *58*, 635–673.